POROSITY PREDICTION USING 3D SEISMIC GENETIC INVERSION AT F3 BLOCK, OFFSHORE NETHERLANDS

Adeoti, L., Bako, M. E., Adeogun, O. Y.,[*] Anukwu, G. C. and Adegbite, T. J.

[1]Department of Geosciences, University of Lagos, Akoka, Lagos, Nigeria.
[*]Corresponding Author's Email: kemmyadesanya@gmail.com

ABSTRACT

Seismic and well information have been incorporated with a genetic inversion workflow using a supervised neural network in the F3 block, offshore Netherlands with a view to properly predicting porosity distribution within the selected reservoirs. This would provide spatial distribution of porosity within the field. Petrophysical parameters were estimated for the identified reservoirs (FS4, FS8, XYZ and ABC) across the four wells (F02-01, F03-02, F03-04 and F03-06) ranging from 780 to 1500 ms. Acoustic impedance (AI) and porosity cubes were generated using a genetic neural network. Thereafter, acoustic and porosity maps were extracted for the selected reservoirs. The results of the inversion reflect that the acoustic impedance in the region varies from 2000 to 6000 kPa.s/m, indicating unconsolidated and less compacted formation within the study area. Porosity within the selected reservoirs varies from 0.25 to 0.40, which reflects very good to excellent porosity values within the study area. The plot of porosity from well (F02-01) and the predicted porosity from genetic inversion reveals a relatively good correlation coefficient of 68%. The hydrocarbon regions within the F3 block are in the Upper Jurassic – Lower Cretaceous strata which are found below the interval available for this study. The study underscores that the genetic inversion algorithm has proven effective in predicting porosity within the study area.

Keywords: Genetic inversion, Porosity cube, Neural network, Acoustic impedance, Reservoir quality.

INTRODUCTION

Reservoir quality depends on the spatial distribution of porosity and permeability of sand and carbonate reservoirs. Both parameters are major players that determine the economic viability of any reservoir for hydrocarbon exploration or exploitation. They therefore need to be quantified in all stages of the life cycle of an oil and gas field; from the basin focus, via appraisal and field development through secondary and tertiary recovery in order to minimize cost and maximize return on investment (Armitage *et al.,* 2018). Porosity is one of the properties that have tremendous impact on reserve estimation and production forecasts. It could be measured in the laboratory from core data or during well testing. Both techniques are expensive however; it could also be estimated from well logs (neutron, density and sonic log). Despite its relevance, challenges still arise when estimating it, majorly because it varies significantly over a reservoir volume and most of the traditional methods only sample it at well locations and not directly across the whole field. Seismic measurements help to delineate geologic structures within the reservoir body but difficult to directly estimate porosity. Inversion is a suitable tool that could be adopted to improve

the spatial prediction of reservoir properties from 3D seismic data (Adeoti *et al.,* 2017; Adesanya *et al.,* 2021). It is capable of incorporating seismic and well information to generate spatial distribution of porosity beyond well controls which is very essential for a successful development plan for hydrocarbon exploration (Bhatt and Helle, 2002; Tiab and Donaldson, 2004; Adekanle and Enikanselu, 2013). Hampson *et al.* (2001) applied neural network for reservoir characterization using a linear and non-linear multi-attributes transform between a subset of the attributes and the target log values. The models generated enhanced interpretation. Likewise, Pavlova and Reid (2010) successfully predicted porosity cubes using genetic inversion, the results assisted in planning for new well locations in Panax's Limestone Coast Geothermal Project. Mojeddifar *et al.* (2015) adopted a pseudo-forward equation (PFE) to generate porosity models of gas reservoir in the F3 block of North Sea. The derived acoustic impedance and porosity were cross plotted with that of well data to validate the PFE model generated which reflected about 93.8% correlation coefficient. Ali and Ahmed (2017) carried out genetic inversion on 3D seismic data to characterise the reservoir for prospects

evaluation in AL-Kumait oil field south Iraq. The results helped to identify the possible locations for exploration development. Li *et al.* (2019) introduced an inversion technique that combines spectral decomposition and genetic inversion. The models generated enhanced interpretation and readjusted tuning effects. Kushwaha *et al.* (2020) used a multi-layer feed-forward neural network (MLFN) to predict porosity by integrating seismic and well data acquired offshore F3 block, Netherlands. The MLFN revealed a relationship between porosity logs and a set of seismic attributes, which in turn were used for porosity prediction. Africa (2021) used genetic inversion and seismic attribute to identify potential hydrocarbon zones and characterised the reservoirs in the Northern Orange basin, offshore South Africa. The need for lateral variation of porosity beyond well controls in the study area is of great concern, though porosity can be estimated from core samples and well log data available. However, these only revealed porosity at the well locations or the zone where core samples were taken, not within the whole field. This informed the application of seismic inversion techniques to predict reservoir porosity within the F3 Block offshore Netherlands (Mojeddifar *et al.,* 2015; Kushwaha *et al.,* 2020). This study adopted genetic inversion algorithm which is simple, fast and reliable to predict the spatial porosity distribution so as to identify new locations for economic decision.

Location and Geology of Study Area
The study area is situated offshore within the Dutch sector of the North Sea, Netherlands. It covers about 380 km^2 and it is characterised by reflectors belonging to the Miocene, Pliocene and Pleistocene with a large-scale sigmoidal deltaic package consisting of sands and shales (Figure 1). Most of the region's hydrocarbons are being sourced by the Upper Jurassic syn-rift, organic-rich marine distribution within the F3 Block for prospect evaluation mudstones (the Kimmeridge Clay Formation) (Brooks *et al.,* 2001). Cretaceous and Cenozoic post-rift thermal subsidence and burial enabled the source rocks to become mature for hydrocarbon generation along the rift axes from Paleogene times onward (Johnson and Fisher, 1998). Hydrocarbon migration in the basin is primarily vertical, but there occurs a significant lateral migration that is however restricted to the Upper Jurassic and Paleogene successions. Almost every clastic and carbonate sedimentary succession, ranging in age from, and including, Devonian and Eocene strata serve as reservoirs for hydrocarbons. Pre-rift producing fields comprise Palaeozoic, Triassic to Lower Jurassic and Middle Jurassic categories (Brooks *et al.,* 2001). The Middle Jurassic tilted fault-block play is best developed in the East Shetland Basin and is one of the most productive in the North Sea. The syn-rift hydrocarbons producing fields display a wide variety of trapping mechanisms, including tilted fault blocks, domes, and stratigraphic closures. Thick, post-rift Lower Cretaceous mudstones serve as regional seals for many of the traps. Mass-flow sandstone reservoirs of Paleogene age are estimated to contain about 20% of the oil province's proven hydrocarbon reserves (Pegrum and Spencer, 1990).

Tectonics	System	Series	Group	Formation	Member	Lithology
Postrift	Quaternary		Nordland			
	Neogene	Pliocene	Westray	Lark		
		Miocene				
	Paleogene	Oligocene	Stronesay	Horda		
		Eocene			Tay	
				Balder		
		Paleocene	Moray	Sele	Forties	
					Mey	
			Montrose	Lista		
				Maureen		
	Cretaceous	Upper	Chalk	Ekofisk		
				Tor		
				Hod		
				Herring		
				Hidra		
		Lower	Cromer Knoll	Rodby		
				Valhall		
Synrift	Jurassic	Upper	Humber	Kimmeridge Clay		
				Heather	Fulmar	
Postrift		Middle	Fladen	Pentland		
	Triassic		Skagerrak		Jonathan Mdst	
		Upper			Joanne Sst	
			Heron		Julius Mdst	
		Middle			Judy Sst	
Synrift		Lower		Smith Bank		
Postrift	Permian		Zechstein	Shearwater Salt		
Synrift			Rotliegendes	Auk		
Synrift	Devonian	Upper	Old Red	Buchan		

Legend:
- Shale
- Tuff
- Chalk
- Sandstone
- Halite

Figure 1: Regional stratigraphy of the Central Graben, North Sea (Stricker and Jones, 2016).

Basic Concept of Genetic Inversion

This technique helps in extracting from the seismic data, the underlying geology which gave rise to seismic data. It is a semi-automatic technique that relies on multi-layered neural networks as well as algorithms that could be used to train selected properties from the well data which would be applied on the seismic volume to generate acoustic impedance cube and thereafter porosity cube. The quality of the inversion products are determined by blind well test which involves the cross plot of predicted porosity with porosity from the well data. The neural workflow is characterised by an activation (sigmoid) function stated in equation 1.

$$f(x) = \frac{1}{1 + e^{-x}}$$

(Veeken *et al.*, 2009) (1)

and an input/hidden-layer relationship:

$$\gamma_{hidden\ layer} = f\left(\sum_{i=1}^{n-1} y_{input,i}.w_{input,i} + w_{input,n}\right).$$

(Veeken *et al.*, 2009)   (2)

In addition, W_n and w_{p+1} represent the bias of the input layer and the bias of the hidden layer, respectively (Veeken *et al.,* 2009).

MATERIALS AND METHODS
Data Gathering
The 3D post-stack time-migrated seismic data

acquired in Netherlands Offshore F3 Block was used in this study (Figure 2). The data set was obtained via the Open Seismic Repository on the OpendTect website. It covers 651 in-lines and 951 cross-lines with time range of 1,848 ms, at sampling rate of 4 ms and bin size of 25 m. The data was acquired in order to explore for oil and gas in the Upper-Jurassic – Lower Cretaceous strata, which are below the interval of the data available for this study that only comprises reflectors belonging to the Miocene, Pliocene and Pleistocene. Along with the 3D seismic data, the repository also provides four wells (F02-01, F03-02, F03-04 and F03-06). Only one well (F02-01) had an effective porosity log. All wells had a density log except well F06-01. Resistivity and neutron logs were absent from all the wells but well tops were available which were used in lithology correlation across the study area. All wells also had check shot log which were used to establish the time-depth relations in the well. The mapped horizons (FS8, FS4, XYZ and ABC) ranging from 780 to 1500 ms guided the genetic inversion. The workflow adopted in this study is displayed in Figure 3.

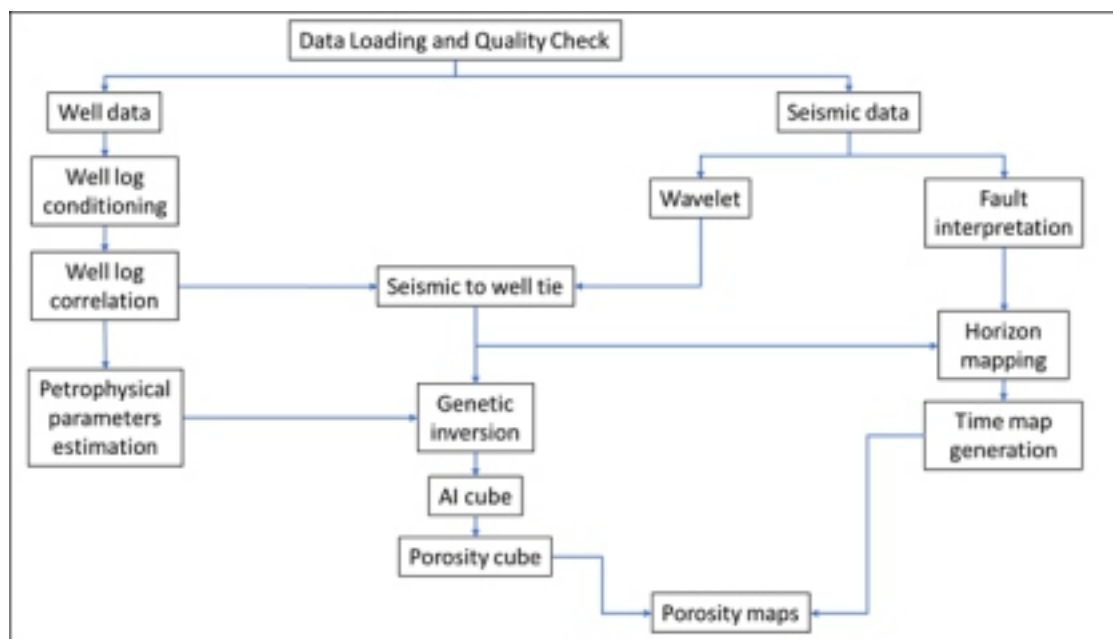**Figure 2:** Base map showing the location of the F3 Block and the available wells.

Figure 3: Workflow adopted in this study.

Well Log Analysis

Gamma ray log was used for lithology discrimination. The high gamma ray response indicates shale formation while low gamma response indicates sand/sandstone formation. Some of the relevant logs required for the study unavailable were computed using empirical formulae stated in equations (3 - 10). The F02-1 logs were used to validate the computed logs.

To compute density log, velocity log had to be computed first from the sonic log using the relationship:

$$V_p = \frac{0.305 * 10^6}{\Delta t} (m/s) \qquad (3)$$

The density log was computed from the velocity log using Gardener's equation, which relates both density, ρ and velocity, V_p by; $\rho = 310 * 10^{-3} * V_p^{0.25}$ (g/cm^3) (Gardener *et al.,* 1974). (4)

Equations (3 and 4) have been modified to factor in unit conversions. The total porosity log was computed from the density log using the sandstone matrix porosity formula:

$$\emptyset_D = \frac{\rho_{ma} - \rho_b}{\rho_{ma} - \rho_f} \qquad (5)$$

Where $\emptyset_D$ = Density-derived porosity ρ_{ma} = sandstone matrix density (2.65 g/cm^3) ρ_b = measured bulk density ρ_f = mud-filtrate density (1.05 g/cm^3)

Firstly, Shale volume (Vsh) was computed according to Clavier *et al.* (1971) equation 6 given by;

$$V_{shale} = 1.7 - \sqrt{3.38 - (GR_{index} + 0.7)^2} \qquad (6)$$

Where $GR_{index} = \dfrac{GR_{log} - GR_{ma}}{GR_{shale} - GR_{ma}}$ (7)

GR_{ma} is a gamma ray log reading in 100% matrix rock, GR_{shale} is a gamma ray log reading in 100% shale, and GR_{log} is a gamma ray log reading in a zone of interest.

The total porosity within the shaly region was calculated using equation 8 according to Oras *et al.* (2019);

$$\emptyset_{t\_shale} = \frac{\rho_{ma} - \rho_{log}}{\rho_{ma} - \rho_f} \qquad (8)$$

Where $\emptyset_{t\text{-}shale}$ = Density-derived shale porosity
ρ_{ma} = shale matrix density (2.54g/cm^3)
ρ_b = measured bulk density

ρ_f = mud-filtrate density (1.05g/cm^3)

The effective porosity was calculated using equation 9 according to Oras *et al.* (2019);

$$\emptyset_{eff} = \emptyset_D - (\emptyset_{t_{shale}} * V_{shale}) \qquad (9)$$

The S-wave velocity log was computed from equation 10 according to Castagna *et al.* (1985):

$Vp = 1.16*Vs+1.36$ or;
$Vs = 0.8621*Vp - !.1724$ (10)

Correlation of Events on Both Seismic and Well Data

Well data which is a point data acquired in 1D, needs to be tied to the seismic data for accurate prediction of reservoir properties such as porosity away from the well bore. To achieve this, check-shot data from well F02-01 was used to establish the time-depth relations for good well-to-seismic tie. The de-spiked sonic and density logs were convolved with a 50 Hz Ricker wavelet to generate an acoustic impedance log from which reflection coefficient sticks were generated, thereafter producing a synthetic seismogram. A good match was observed after 5 ms bulk shift which gave 52.6% correlation coefficient.

Fault and Horizon Picking

After a successful seismic to well tie, faults were picked on seismic cube by observing areas of reflection discontinuity and displacement of fault blocks at the fault plane, as well as relative termination or change in pattern of reflection events. Afterwards, the reservoir tops of interest (FS8, FS4, XYZ and ABC) ranging from 780 to 1500 ms were identified and mapped across the seismic cube.

Genetic Inversion

The AI inversion was driven by genetic algorithm which allowed the selection of optimum parameters for quality inversion products. The F3 seismic data was integrated with well data from (F03-02, F03-04 and F03-06) guided by mapped horizons (FS8, FS4, XYZ and ABC) ranging from 780 to 1500 ms to generate inverted AI. The inverted AI was then plotted against the AI from the well data as a quality check. After the generation of the inverted AI cube, the porosity cube was then generated according to (Veeken *et al.,* 2009). The predicted porosity was then plotted

against the porosity from well (F02-01) as a quality check. The step by step procedure for the genetic inversion is displayed in Figure 4.

Figure 4: Genetic Inversion workflow (modified from Veeken *et al., 2009*).

RESULTS AND DISCUSSION
Derived Logs and Well Correlation

The derived logs are displayed in Figures 5 and 6. Figure 7 is the cross plot of computed density log and density log from well (F02-01) with correlation coefficient of 99% while Figure 8 is the cross plot of the computed effective porosity and effective porosity from well (F02-01) with correlation coefficient of 100%. These values validate the equations and parameters used in the well log analysis.
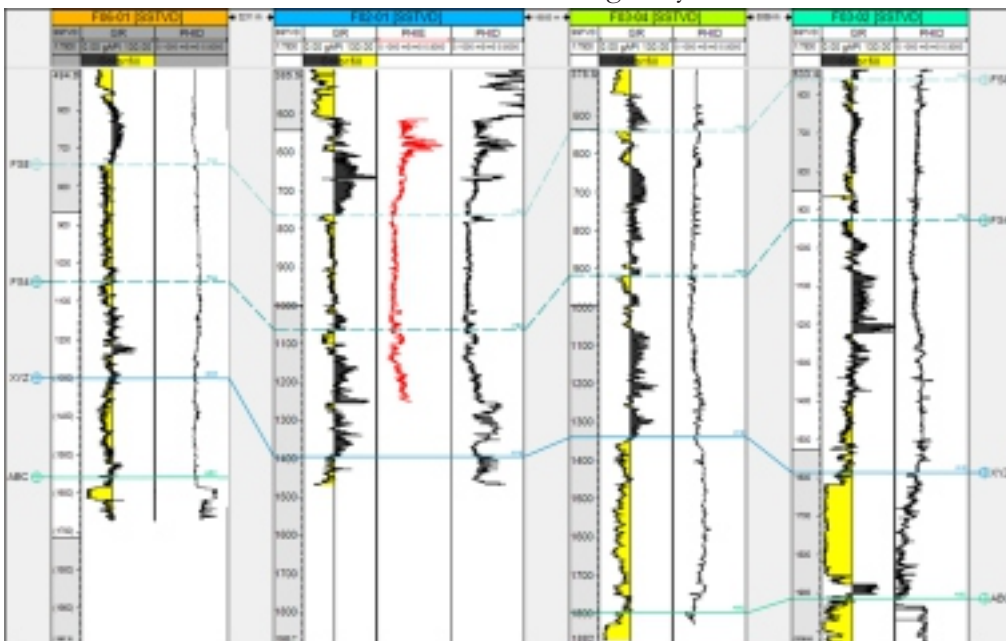
Figure 5: Derived total porosity logs (PHID) from density logs.
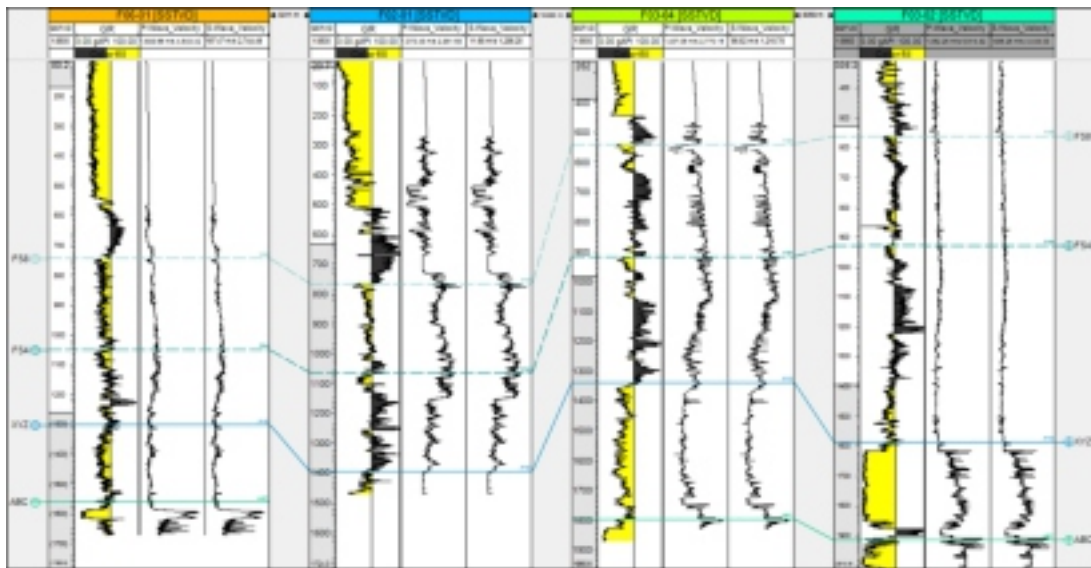
Figure 6: Derived Vp and Vs logs for all the wells.
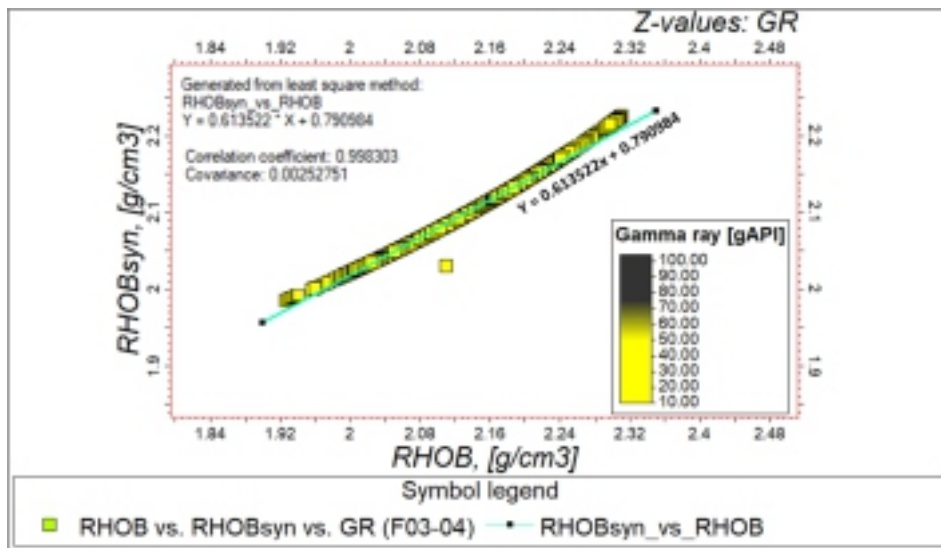
Figure 7: Cross plot of computed density log (RHOBsyn) and density log (RHOB) for well (F02-01).
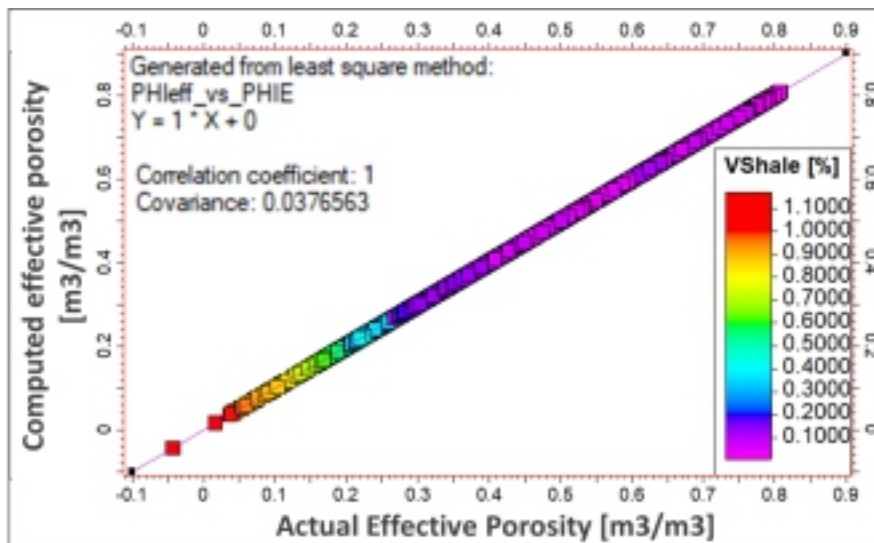
Figure 8: Cross plot of computed effective porosity and effective porosity for well (F02-01).

Figure 9 shows the correlation of selected reservoirs across the wells (F02-01, F03-02, F03-04 and F03-06) using gamma ray log. The well logs indicate that the transparent facies are of standardized lithology that can either be sand or shale. The sands are seen to thin out in the basin ward direction indicating a change in facies from coarse-grained deposits at the proximal part of the basin to finer-grained deposits at the distal part.
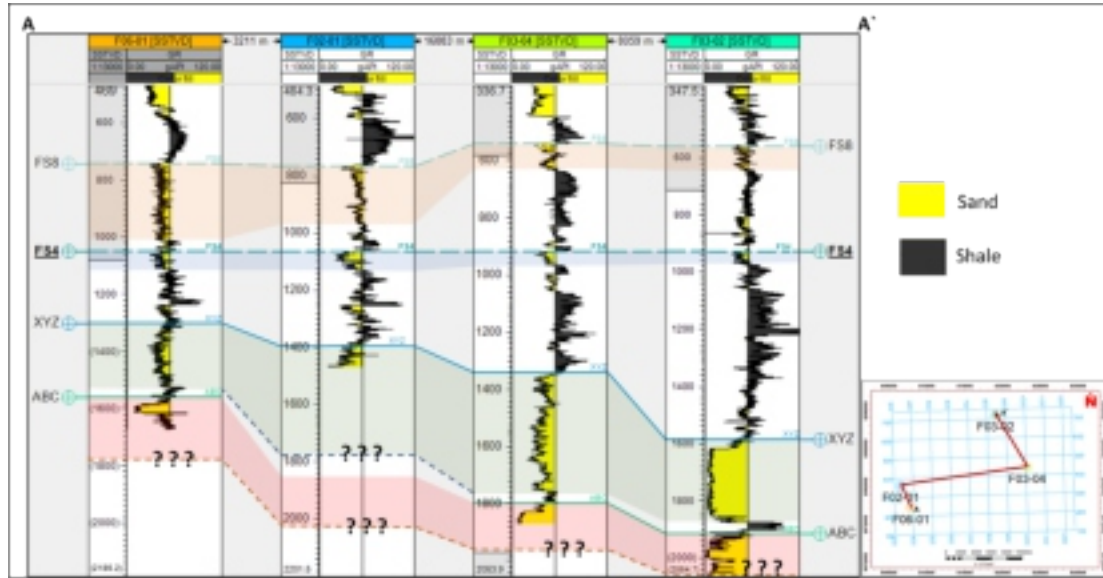
Figure 9: Correlation of reservoir tops across the four wells.

Mapped Faults and Horizons

After a successful seismic to well tie (Figure 10) with 52.6% correlation coefficient. A major fault trending in the NE-SW direction was identified with fourteen minor faults. These faults immensely have significant effect on the geology of the area (Figure 11). Five reservoir tops (FS8, FS4, XYZ and ABC) ranging from 780 to 15000 ms were identified and mapped. The structural time maps were generated based on the mapped horizons (FS8, FS4, XYZ and ABC) as displayed in Figure 12 (a–d) which revealed structural closures and associated faults. The reservoir FS8 which occurs at a depth of about 500 m shows structural closures at the northeastern region that is associated with minor faulting occurring at that area. Reservoir FS4 at depth of about 900 m reveals no structural closures while reservoir XYZ at 1350 m shows two closures at the northeastern and the southeastern areas, with the latter representing the top of a faulted anticline. Reservoir ABC occurs at a depth of 1800 m and shows a well-developed anticline that has been greatly faulted. Minor faults are also observed to occur in the southwestern parts of the reservoir. Reservoir ABC also pinches out north of the study area.
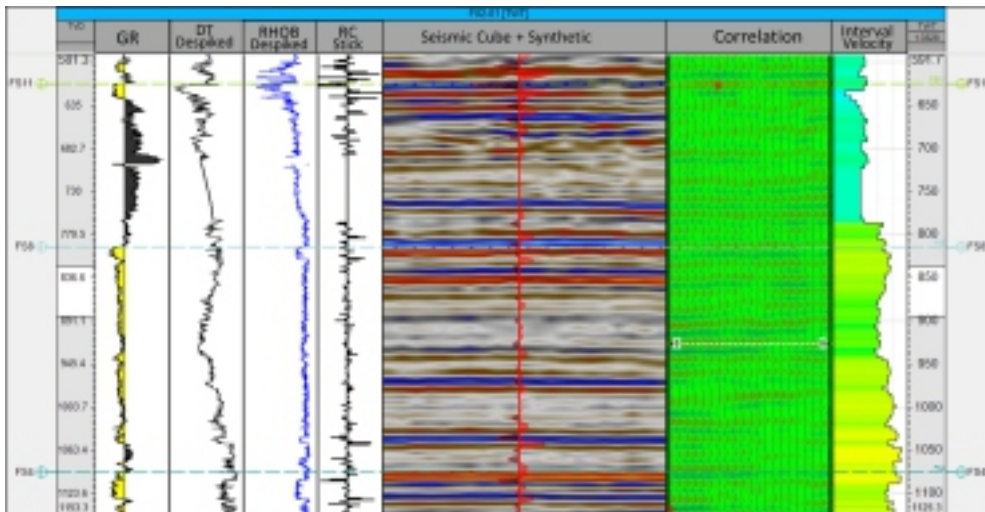
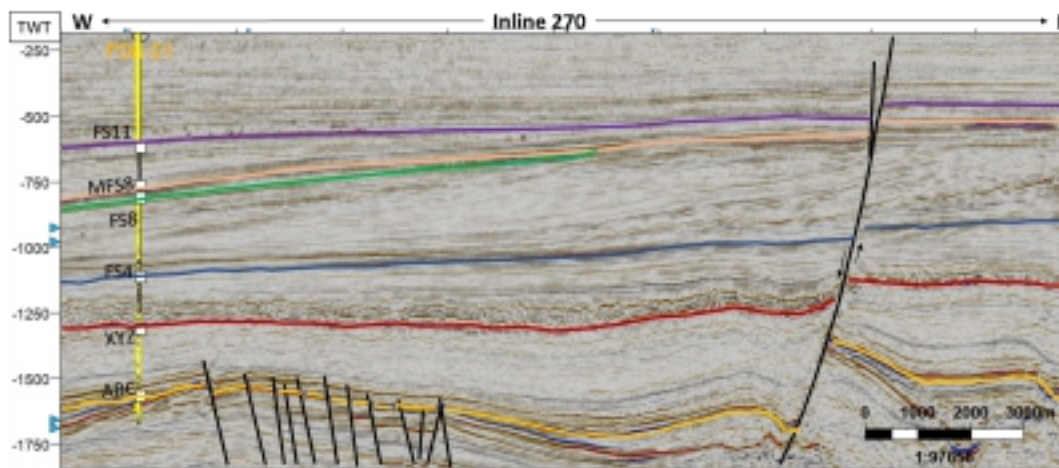**Figure 10**: Correlation of events on both Seismic and well data.

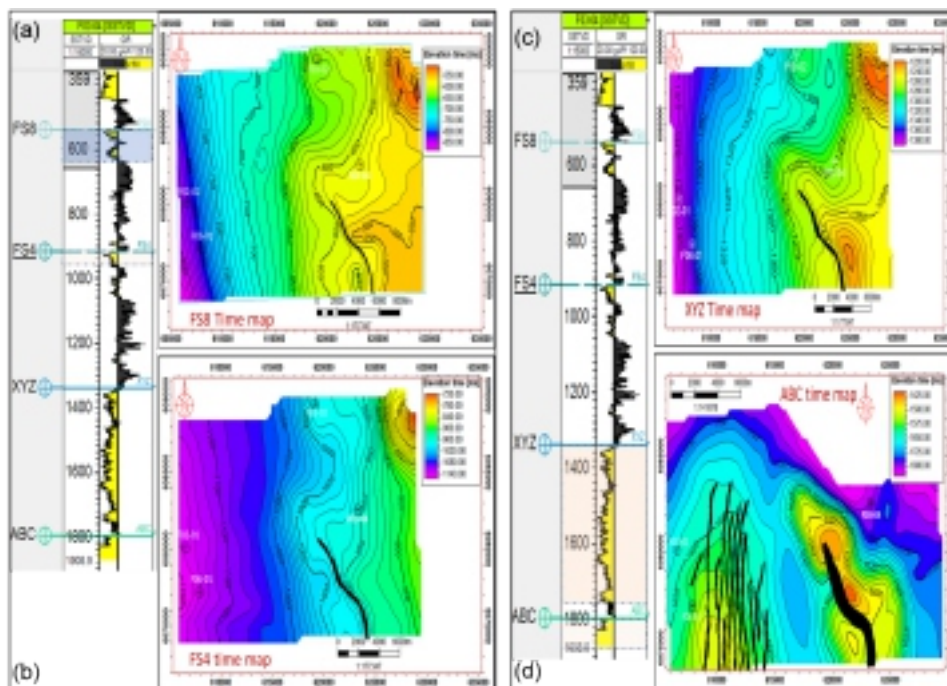**Figure 11:** Mapped faults and horizons.

Figure 12 (a-d): Time structural map of the reservoirs of interest (FS8, FS4, XYZ and ABC).

Inverted Acoustic Impedance Cube

Figure 13 shows high match between the inverted AI cube and inserted AI log from the well (F03-04) while Figure 14 is the cross plot of the inverted AI and AI from well (F02-01) with correlation coefficient of 96%. The inverted AI cube shows impedance variation of 2000 to 6000 kPa.s/m. The observed associated low impedance indicates presence of unconsolidated sand formation.
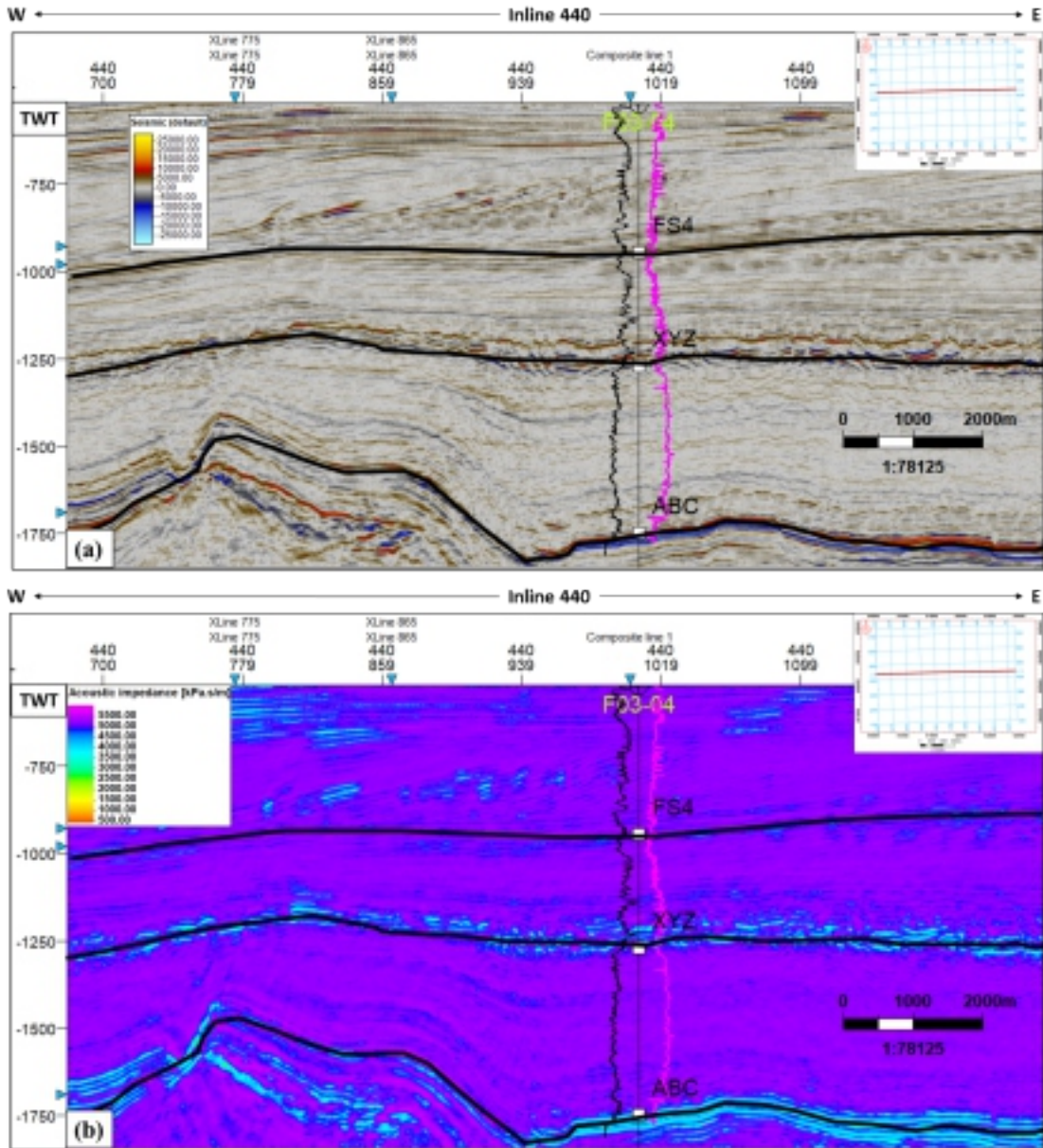

Figure 13: Inline 440 showing GR log (black) and AI log (pink) from well (F03-04) on (a) seismic cube (b) inverted AI cube.
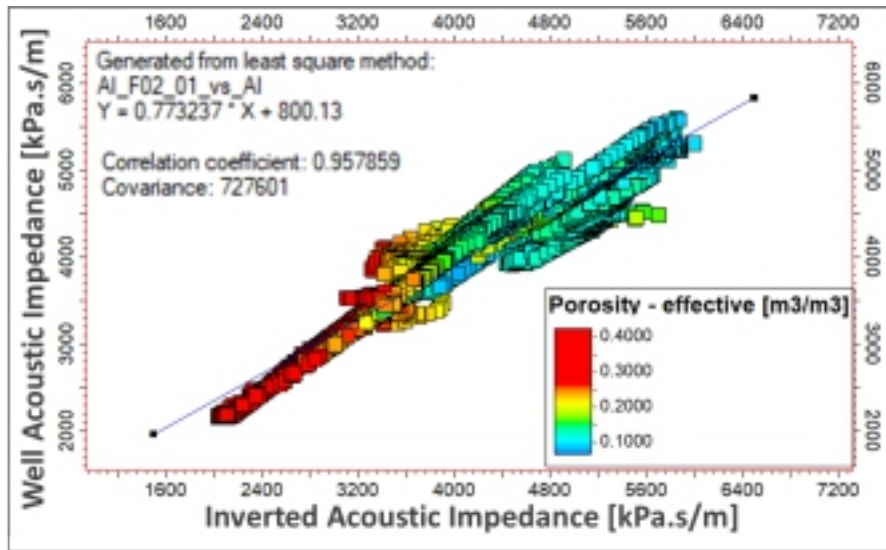
Figure 14: Cross plot of inverted AI and AI from well (F02-1).

Predicted Porosity

Figure 15 is the predicted porosity cube which reveals the spatial distribution of porosity ranging from 0.1 to 0.48 while Figure 16 is the cross plot of the predicted porosity and porosity from well (F02-01) with correlation coefficient of 68%, this indicates good prediction and it equally agrees with findings of (Kushwaha *et al.,* 2020).
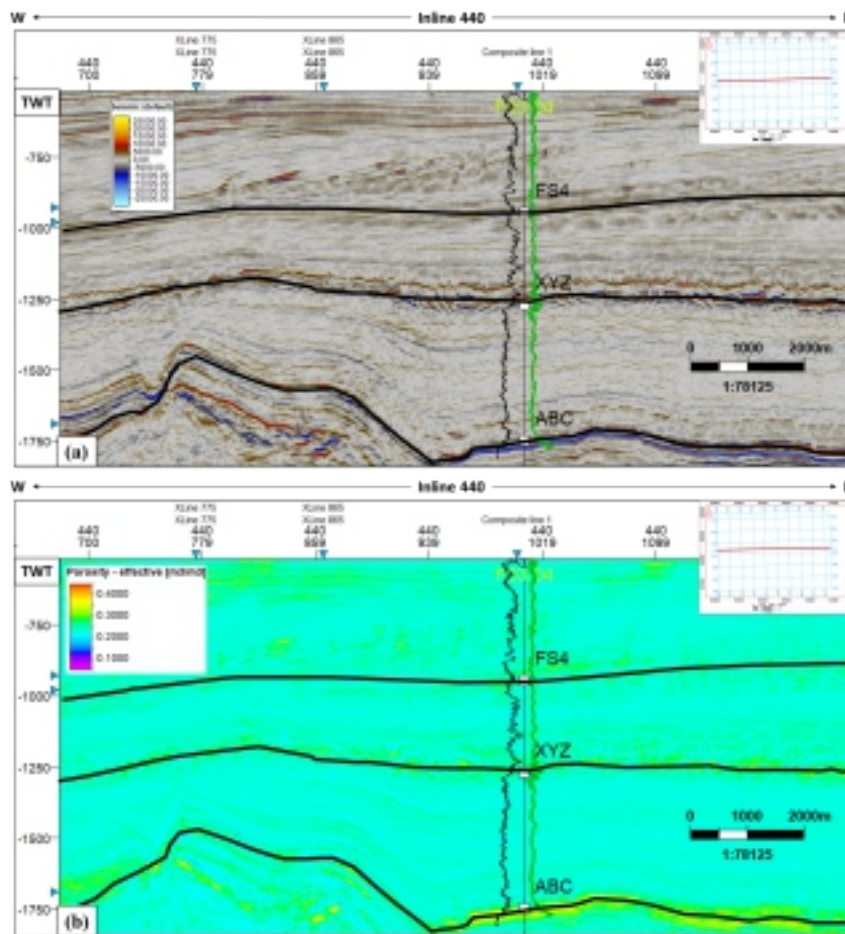

Figure 15: Inline 440 showing GR log (black) and porosity log (green) from well (F03-04) on (a) seismic cube (b) predicted porosity cube.
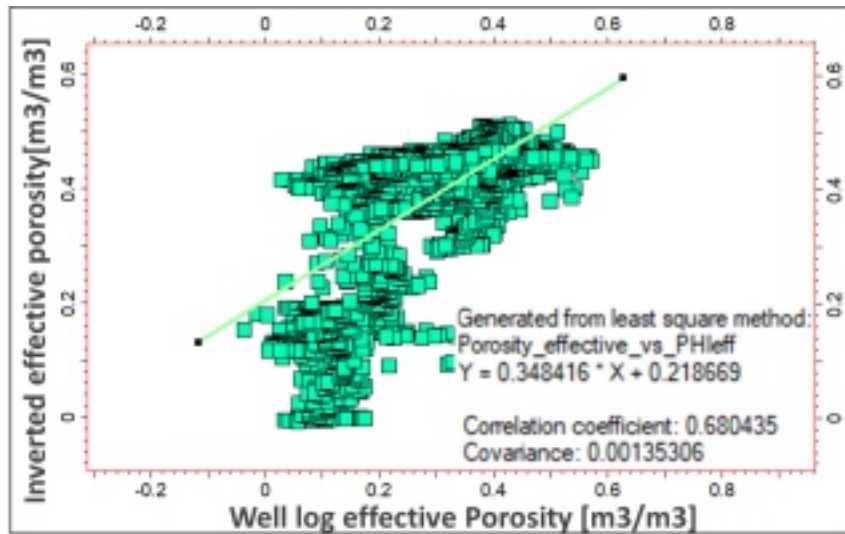
Figure 16: Cross plot of predicted porosity and porosity from well (F02-01).

Extracted AI and Porosity Maps from Top of Reservoirs (FS8, FS4, XYZ and ABC)

The extracted AI map at time slice 1692 ms (Figure 17) shows good inverted AI distribution across the field. The AI slice reflects yellow to green colour indicating low AI sand (3000 kPa.s/m) compared to the background purple indicating high AI (6000 kPa.s/m) sand/shale.
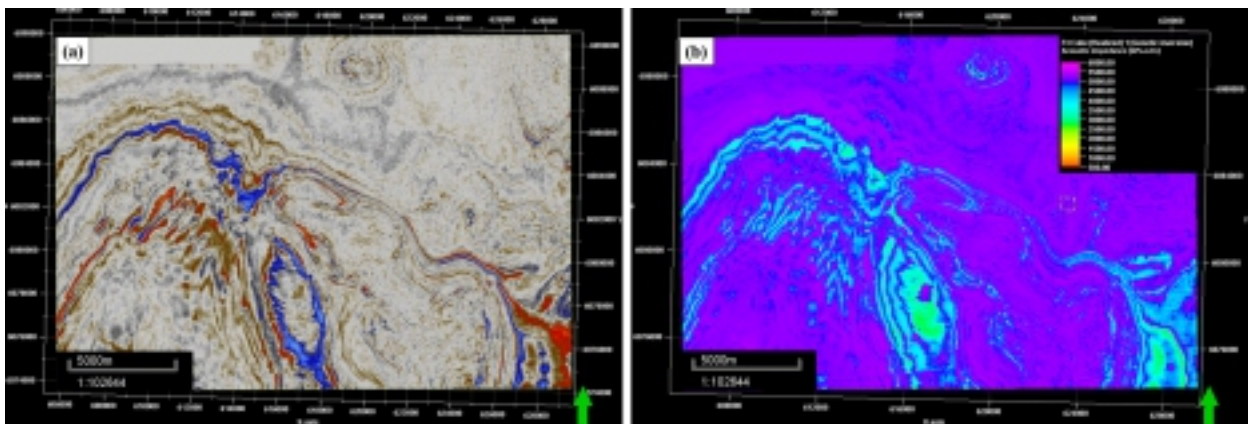

Figure 17: 2D window showing (a) seismic cube (b) inverted AI Cube at time slice 1692 ms

The extracted porosity map at time slice 1692 ms (Figure 18) shows good porosity distribution across the field with little changes in porosity laterally and vertically. The variation of porosity across the reservoirs is between 0.25 – 0.40, which is comparatively high thereby confirming that the area is unconsolidated formation. There seems to be no preferred pattern of porosity distribution across the maps (Figures 20 & 21), except reservoir ABC which seems to have very low values just at the north-eastern boundaries.
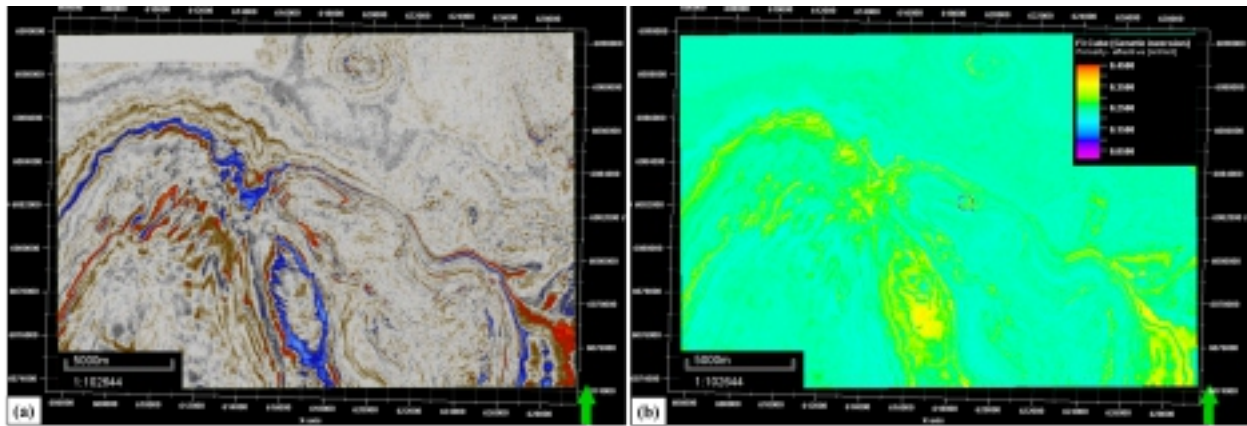
Figure 18: 2D window showing (a) seismic cube (b) generated porosity cube at time slice 1692 ms
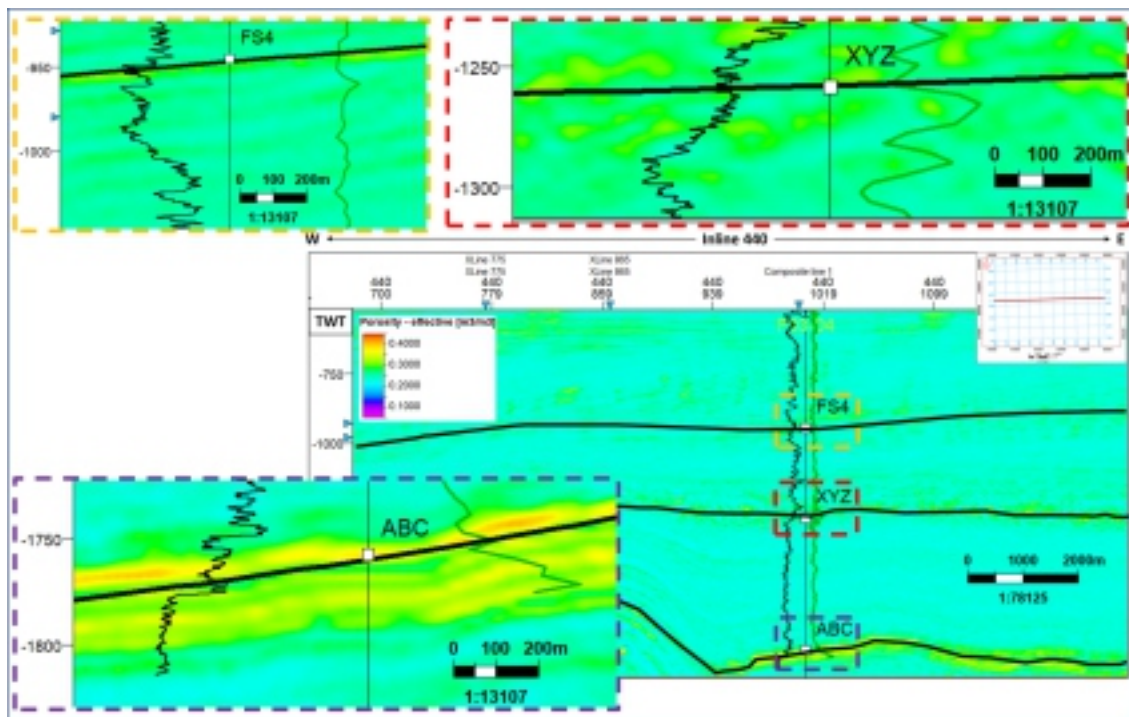

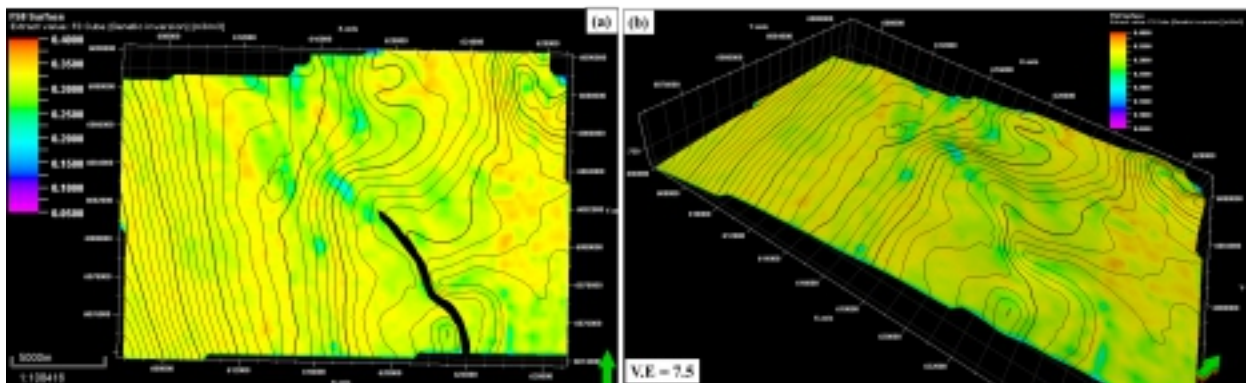**Figure 19:** Response of the porosity logs at the reservoirs.

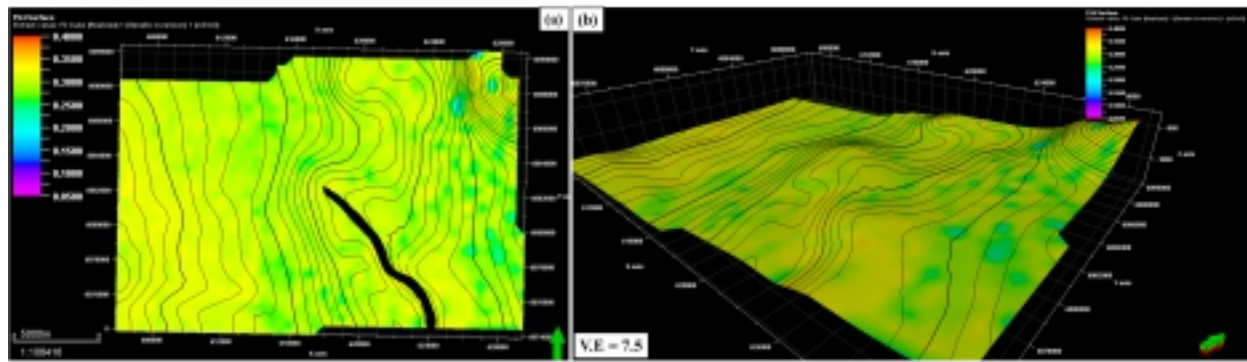**Figure 20:** Reservoir FS8 porosity map on (a) 2D window (b) 3D window.

Figure 21: Reservoir FS4 porosity map on (a) 2D window (b) 3D window.

CONCLUSIONS

In this study, reservoir porosity has been predicted from the genetic inversion of offshore seismic data incorporated with well data of F3 Block, Netherlands. Four reservoirs (FS8, FS4, XYZ, and ABC) were identified from the wells and thus mapped across the entire field. The missing petrophysical logs (density, Vs, Vp, porosity, AI) in some wells were computed using relevant equations. The predicted AI and porosity cubes were validated by blind well test. This involves the cross plot of predicted AI and AI from well (F-02-01) and plot of predicted porosity and porosity from well (F-02-01). The plots revealed 96% and 68% correlation coefficient respectively. These indicate good predicted AI and porosity cube. The porosity maps extracted at top of reservoirs (FS4, FS8, XYZ and ABC) reveal the spatial distribution of porosity across the field ranging from 0.25 to 0.4 described as very good to excellent porosity. These extracted porosity maps can guide well placement for development plans. However, the hydrocarbon regions within the F3 block are in the Upper Jurassic – Lower Cretaceous strata which are found below the interval available for this study. Hence, the method deployed in this study has shown the effectiveness of the technique in predicting porosity away from the well.

ACKNOWLEDGEMENTS

The authors want to say a big thank you to Earth Signature Research Group of University of Lagos for the support rendered. Also, we appreciate the opportunity to access dataset via Open Seismic Repository on the OpendTect Website.

CONFLICT OF INTEREST

The authors declare that there is no conflict of interest in the course of research.

REFERENCES

Adeoti, L., Adesanya, O.Y., Oyedele, K.F., Afinotan, I.P. and Adekanle, A., 2017. Lithology and fluid prediction from simultaneous seismic inversion over Sandfish field, Niger Delta. Nigeria. *Geosciences Journal,* 10:1–15.
doi: 10.1007/s12303-017-0018-4

Adekanle, A. and Enikanselu, P.A., 2013. Porosity prediction from seismic inversion properties over 'XLD' Field, Niger Delta. *American Journal of Scientific and Industrial Research,* 4:31–35.
doi: 10.5251/ajsir.2013.4.1.31.35

Adesanya, O.Y., Adeoti, L., Oyedele, K.F., Afinotan, I.P., Oyeniran, T. and Alli, S., 2021. Hydrocarbon reservoir delineation using simultaneous and elastic impedance inversions in a Niger Delta field. *Journal of Petroleum Exploration and Production Technology,* 1:1–15.
doi: 10.1007/s13202-021-01191-5

Africa, R., 2021. Reservoir Delineation and Characterization in the Northern Orange Basin, using Genetic Inversion and Seismic Attribute. Proceedings of EAGE 5th Eastern Africa Petroleum Geoscience Conference held online March 1 –5.
doi: 10.3997/2214-4609.2021605006

Ali, M.A. and Ahmed, A.A., 2017. 3D Seismic Genetic Inversion for Reservoir Characterization and Prospects Identification. *International Journal of Science and Research (IJSR) ISSN (Online):* 2319–7064.
doi: 10.21275/ART20177226

Armitage, P.J., Butcher, A.R., Churchill, J.M., Csoma, A.E., Hollis, C., Lander, R.H., Omma, J.E. and Worden, R.H., 2018. Reservoir Quality of Clastic and Carbonate Rocks: Analysis, Modelling and Prediction, *Geological Society, London, Special Publications,* 435:1–31.
doi: 10.1144/SP435

Bhatt, A. and Helle, H., 2002. Determination of facies from well logs using modular neural networks. *Petroleum Geosciences,* 8: 217–228.
doi: 10.1144/petgeo.8.3.217

Brooks, J.R.V., Stoker, S.J. and Cameron, T.D.J., 2001. Hydrocarbon exploration opportunities of the twenty-first century in the United Kingdom. In: Petroleum Provinces of the Twenty-First century (Eds. Downey, M.W.; Threet, J.C.; Morgan, W.A.). Boulder CO, USA, AAPG, 167-199, 573pp. /AAPG Memoir, 74

Castagna, J.P., Batzle, M.L. and Eastwood, R.L., 1985. Relationship between compressional wave and shear wave velocities in clastic silicate rocks, *Geophysics,* 50: 571–581.
doi: 10.1190/1.1441933

Clavier, C., Hoyle, W. and Meunier, D., 1971. Quantitative interpretation of thermal neutron decay time logs: part I. Fundamentals and techniques, *Journal of Petroleum Technology,* 23(6): 743–755.
doi: 10.2118/2658-A-PA

Gardner, G.H.F., Gardner, L.W. and Gregory, A.R., 1974. Formation velocity and density—the diagnostic basics for stratigraphic traps, *Geophysics*, 39:770–780.
doi: 10.1190/1.1440465

Hampson, D.P., Schuelke, J.S. and Quirein, J.A., 2001. Use of multi attribute transforms to predict log properties from seismic data, *Geophysics,* 66: 220–239.
doi: 10.1190/1.1444899

Johnson, H.D. and Fisher, M.J., 1998. North Sea plays: geological controls on hydrocarbon distribution. In: Petroleum geology of the North Sea, basic concepts and recent advances (Eds. Glennie, K.W.) 4th edition: London, Blackwell Science Limited, pp. 463–547.
doi: 10.1002/9781444313413.ch12

Kushwaha, P.K., Maurya, S.P., Rai, P. and Singh, N.P., 2020. Porosity prediction from offshore seismic data of F3 Block, the Netherlands using multi-layer feed-forward neural network, *Current science,* 19: 10.
doi: 10.18520/cs/v119/i10/1652-1662

Li, W., Yue, D., Wu, S., Wang, W., Li, J., Wang, W. and Tian, T., 2019. Characterizing meander belts and point bars in fluvial reservoirs by combining spectral decomposition and genetic inversion, *Marine and Petroleum Geology,* 105:168–184.
doi: 10.1016/j.marpetgeo.2019.04.015

Mojeddifar, S., Kamali, G. and Ranjbar, H., 2015. Porosity prediction from seismic inversion of a similarity attribute based on a pseudo-forward equation (PFE): a case study from the North Sea Basin, Netherlands. *Petetroleum Science,* 12:428–442.
doi: 10.1007/s12182-015-0043-8

Oras, J. M., Erik, S. and Jon, K., 2019. Petrophysical interpretation in shaly sand formation of a gas field in Tanzania, *Journal of Petroleum Exploration and Production Technology,* 10:1201–1213.
doi: 10.1007/s13202-019-00819-x

Pavlova, M.A. and Reid, I., 2010. Geophysical inversion of 3D seismic data in Panax's limestone coast geothermal project to determine reservoir porosity. Proceedings of the World Geothermal Congress held in Bali, Indonesia, August, 25-29

Pegrum, R.M. and Spencer A.M., 1990. Hydrocarbon plays in the northern North Sea Statoil, Forushagen (UND-GE), Postboks 300, Stavanger, Norway 4001
doi: 10.1144/GSL.SP.1990.050.01.27

Stricker, S. and Jones, S.J., 2016. Enhanced porosity preservation by pore fluid overpressure and chlorite grain coatings in the Triassic Skagerrak, Central Graben, North Sea, UK. *Geological Society London Special Publications.*
doi: 10.1144/SP435.4

Tiab, D. and Donaldson, E.C., 2004. Petrophysics*:* Theory and practice of measuring of reservoir rocks. 2nd edition, Gulf professional publishing, Oxford 881 pp.

Veeken, C.H., Ampilov, Y. and Priezzhev II, 2009.
Nonlinear multitrace genetic inversion
applied on seismic data across the
Shtokman field, offshore northern Russia.
Geophysics special issue 74:6.
doi: 10.1190/1.3223314